NANO LETTERS

2009
Vol. 9, No. 12
4320-4325

Plasmonic Lens Made of Multiple Concentric Metallic Rings under Radially Polarized Illumination

Weibin Chen,[†] Don C. Abeysinghe,[‡] Robert L. Nelson,[§] and Qiwen Zhan*[,†]

Electro-Optics Graduate Program, University of Dayton, 300 College Park, Dayton Ohio 45469, Department of Electrical and Computer Engineering, University of Cincinnati, Cincinnati, Ohio 45219, and Air Force Research Laboratory, Wright-Patterson Air Force Base, Dayton, Ohio 45433

Received August 5, 2009

ABSTRACT

Optimal plasmonic focusing can be achieved through matching the rotational symmetry of the plasmonic lens to the polarization symmetry of a radially polarized illumination. In this letter, we report the experimental confirmation of the focusing properties and field enhancement effect of plasmonic lens made of multiple concentric annular rings using a collection mode near field scanning optical microscope. Surface plasmons excited at all azimuthal directions propagate toward the geometric center and constructively interfere at the focus to create a strongly enhanced evanescent optical "needle" field that is substantially polarized vertically to the plasmonic lens surface. The field enhancement factor can be improved through adding more rings while maintaining the plasmonic focal spot size. Strategy for optimizing the field enhancement factor is studied with both analytical and numerical methods.

Surface plasmons are collective oscillations of free electrons that can be excited by transverse-magnetic (TM) polarized light at dielectric/metal interface. The surface plasmon waves are associated with shorter effective wavelengths and strong field enhancement effects, making them very attractive for a variety of applications. Because of its shorter effective wavelength, surface plasmon wave can be focused into a highly confined spot with size beyond the diffraction limit, finding applications in many areas such as subwavelength optics,[1,2] super-resolution imaging,[3−5] nanolithography,[6] high harmonic generation,[7] waveguiding,[8] near-field imaging and sensing.[9] The challenges these applications face are the manipulation of the spot size, shape, and strength of the surface plasmon field through designing appropriate optical excitation geometry and plasmonic structures. Plasmon focusing with linearly polarized illumination usually resulted in a minimum longitudinal field at the geometric focus due to destructive interference between counter-propagating surface plasmon waves and an inhomogeneous plasmon focal spot owing to the symmetry mismatch between the incident polarization and the plasmonic structures.[10,11]

It has been demonstrated both numerically and experimentally that optimal plasmonic focusing can be achieved through using a combination of radially polarized illumination and axially symmetric plasmonic structures.[12−16] Nanoscale focal spot with enormous field enhancement can be achieved with such a match in polarization and structure symmetry.[14] Radially polarized beam is one type of cylindrical vector beams whose local electrical field is linearly polarized along the radial directions. It has been demonstrated that radially polarized beam can be focused into a spot smaller than the diffraction limit with high numerical aperture (NA) objective lens owing to its special polarization symmetry.[17−19] If radially polarized beam is focused onto axially symmetric plasmonic structures, unlike linearly polarized beams, the entire beam is TM polarized with respect to the structure, enabling surface plasmon excitation from all directions and homogeneous plasmon focusing through constructive interference of these plasmon waves. More interestingly, due to the angular selection of the SPR, the plasmonic focus generated this way can be an evanescent nonspreading Bessel beam.[12,15]

In this letter, we explore the experimental confirmation of optimal plasmonic focusing properties of multiple annular metallic rings under radially polarized illumination. By making circular subwavelength slit into a silver film, the plasmon waves excited at the edges of the slit will have a curved wavefront and be focused toward the geometrical center. Surface plasmons excited at all azimuthal directions interfere with each other constructively and create a strongly

* To whom correspondence should be addressed. E-mail: qiwen.zhan@notes.udayton.edu.
[†] University of Dayton.
[‡] University of Cincinnati.
[§] Wright-Patterson Air Force Base.

10.1021/nl903145p CCC: $40.75
Published on Web 10/30/2009

Report Documentation Page

Form Approved
OMB No. 0704-0188

Public reporting burden for the collection of information is estimated to average 1 hour per response, including the time for reviewing instructions, searching existing data sources, gathering and maintaining the data needed, and completing and reviewing the collection of information. Send comments regarding this burden estimate or any other aspect of this collection of information, including suggestions for reducing this burden, to Washington Headquarters Services, Directorate for Information Operations and Reports, 1215 Jefferson Davis Highway, Suite 1204, Arlington VA 22202-4302. Respondents should be aware that notwithstanding any other provision of law, no person shall be subject to a penalty for failing to comply with a collection of information if it does not display a currently valid OMB control number.

1. REPORT DATE **05 AUG 2009**	2. REPORT TYPE	3. DATES COVERED **00-00-2009 to 00-00-2009**
4. TITLE AND SUBTITLE **Plasmonic Lens Made of Multiple Concentric Metallic Rings under Radially Polarized Illumination**		5a. CONTRACT NUMBER 5b. GRANT NUMBER 5c. PROGRAM ELEMENT NUMBER
6. AUTHOR(S)		5d. PROJECT NUMBER 5e. TASK NUMBER 5f. WORK UNIT NUMBER
7. PERFORMING ORGANIZATION NAME(S) AND ADDRESS(ES) **Electro-Optics Graduate Program,University of Dayton,300 College Park,,Dayton,OH,45469**		8. PERFORMING ORGANIZATION REPORT NUMBER
9. SPONSORING/MONITORING AGENCY NAME(S) AND ADDRESS(ES)		10. SPONSOR/MONITOR’S ACRONYM(S) 11. SPONSOR/MONITOR’S REPORT NUMBER(S)
12. DISTRIBUTION/AVAILABILITY STATEMENT **Approved for public release; distribution unlimited**		
13. SUPPLEMENTARY NOTES		
14. ABSTRACT		
15. SUBJECT TERMS		

16. SECURITY CLASSIFICATION OF:			17. LIMITATION OF ABSTRACT	18. NUMBER OF PAGES	19a. NAME OF RESPONSIBLE PERSON
a. REPORT	b. ABSTRACT	c. THIS PAGE			
unclassified	**unclassified**	**unclassified**	**Same as Report (SAR)**	**6**	

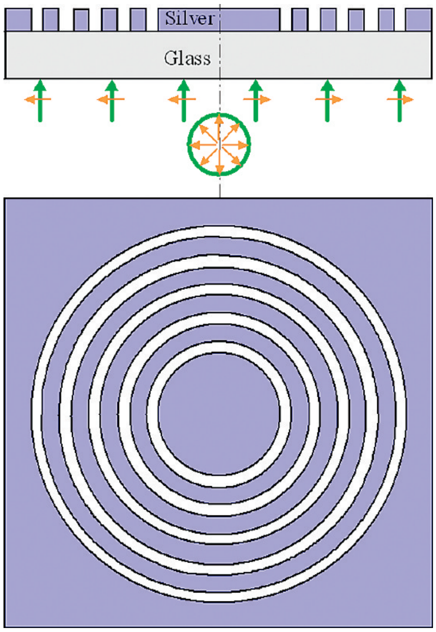

Figure 1. Schematic diagram of plasmonic lens with concentric annular rings structure. Radially polarized light illuminates from the glass substrate side. Because of the rotational symmtry of both the plasmonic lens and excitation geometry, optimal focal spot can be achieved at the center.

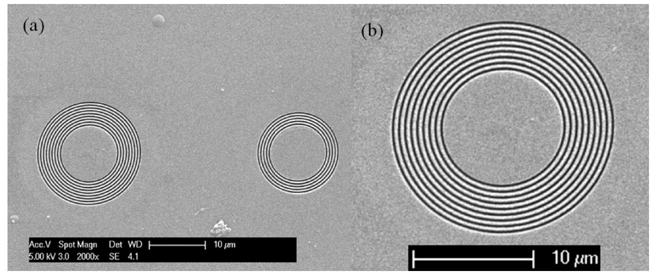

Figure 2. SEM image of (a) 5-ring and 9-ring plasmonic lenses in silver film, and (b) zoom-in of the 9-ring plasmonic lens fabricated with FIB milling.

enhanced localized field at the focus with spot size beyond the diffraction limit. Two-dimensional (2D) intensity distributions at the surface of plasmonic lenses with different number of annular rings are mapped by a collection mode near field scanning optical microscope. Our experimental results confirm that the field enhancement can be increased with additional annular rings while maintaining the plasmonic focal spot size.

The diagram of the experimental setup is illustrated in Figure 1. A radially polarized beam was generated through coupling a charge +1 vortex beam into a few-mode fiber with high efficiency and stability.[15] The optical excitation wavelength was chosen to be 532 nm. A 200 nm silver film was deposited onto a glass substrate by e-beam evaporation. This thickness was chosen to prevent far field direct transmission of the laser through the silver layer. Annular ring patterns with single ring, 5-ring, and 9-ring were fabricated with focused ion beam milling (FIB, FEI dual beam SEM-FIB NOVA 200 Nanolab system). The FIB was used with an acceleration voltage of 30 kV and a very small ion current of 28 pA to obtain the smallest possible beam diameter (21 nm), thus to guarantee minimal redeposition of Ga in the cut regions and highly vertical sidewalls. Figure 2 shows the SEM images of 5-ring and 9-ring plasmonic lenses fabricated in silver film as examples. The innermost ring has a diameter of 9.2 μm. The slit width is 135 nm, and period is 500 nm, which matches to the surface plasmon wavelength. Surface plasmons excited at different slits will have propagation phase differences of $2\pi \cdot n$ ($n = 1, 2, 3...$). Therefore, these surface plasmon waves are in phase and constructively interfere with each other at the geometrical center, producing stronger field enhancement than the single ring plasmonic lens. The surface plasmon intensity distribution is directly imaged by a collection mode NSOM (Veeco Aurora 3) using metal-coated fiber probe with a normal aperture size of 50−80 nm. The fiber probe is mounted on a tuning fork and shear force feedback mechanism is applied to regulate the probe/sample distance.

Because of the rotational symmetry of both the annular metallic rings and optical excitation geometry, surface plasmons excited by the plasmonic lens at all azimuthal directions interfere constructively. Therefore, a tightly focused plasmonic field with strong field enhancement is obtained at the center. There are two components contributing to the total energy density distribution $|E|^2$, namely the longitudinal component $|E_z|^2$ and radial component $|E_r|^2$. $|E_z|^2$ is calculated to be 31.4 times higher than $|E_r|^2$, and dominates the total energy density distribution. The measured 2D intensity distribution of surface plasmon focusing along the air/silver interface of the single ring plasmonic lens shows the expected rotational symmetry (Figure 3a). The surface plasmon waves excited at all azimuthal directions propagate toward the geometric center, creating a strongly enhanced local field due to constructive interference. The focusing effect can be clearly seen as the surface plasmon interference fringes getting stronger when they are closer to the geometrical focus. Because of the symmetry of fundamental mode in the fiber core of the NSOM probe, the detected signal of the apertured NSOM fiber probe is proportional to $|\nabla_\perp E_z|^2$.[11,20] Consequently, the experimental results show a dark center as predicted by the theoretical calculation.[13,15] It is worth noting that our near-field scanning image is rather different from that reported previously.[16] We attribute this difference to the fairly big probe aperture and large scanning distance away from the surface used in ref 16. The transverse profiles of the measured energy density distribution and the numerically computed results with a finite element method model on the silver/air interface are plotted in Figure 3b, showing excellent agreement. The two peaks are about 294 nm apart, which corresponds to a full width half-maximum (fwhm) spot size of 184.4 nm (λ/2.88). The surface plasmon interference fringe period is measured to be 255 nm, in good agreement with theoretical prediction.

The field enhancement of single ring plasmonic lens is given by the constructive interference of surface plasmon waves excited at all azimuthal directions. It is possible to further increase the focal field strength through appropriately

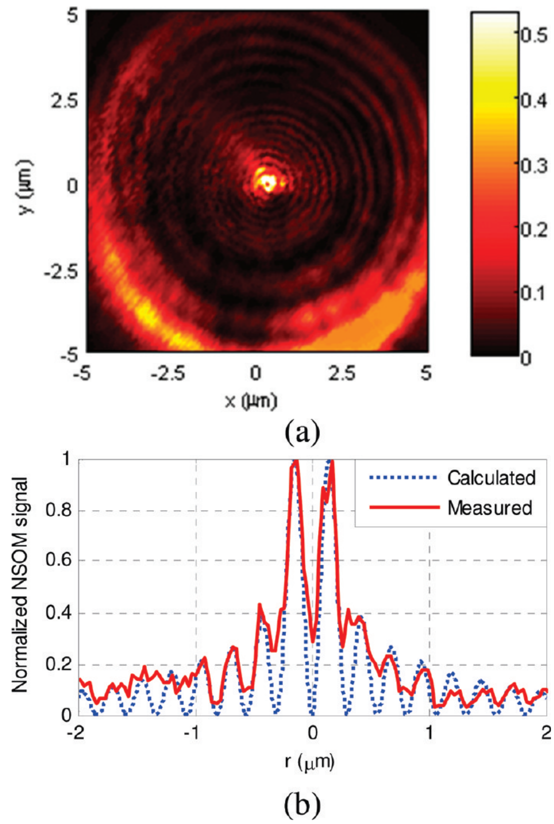

Figure 3. (a) Measured near-field energy density distribution at the air/silver interface for single ring plasmonic lens. Multiple fringes corresponding to surface plasmon wave propagation are observed. Because of the apertured NSOM probe is more sensitive to $|\nabla_{\perp}E_z|^2$, a dark center is obtained as expected. (b) Comparison of measured and calculated transverse profiles of the energy density distribution. Experimental result agrees with the simulation very well.

designing more concentric rings in the plasmonic lens structure. For the multiple concentric rings structure, if the locations of the additional rings are chosen to satisfy the circular Bragg condition for the plasmonic wavelength, then the peak intensity of the plasmonic focus gets stronger while the focal spot remains approximately the same size as more rings are added to the plasmonic lens structure. This is successfully confirmed by the experimental results. Figure 4a,b shows the 2D surface plasmon energy density distributions at the surface of plasmonic lenses with 5-ring and 9-ring patterns, respectively. It is observed that the peak intensity increases with respect to the number of rings. The peak intensity at the plasmonic lens focus for 5-ring and 9-ring plasmonic lenses is 8.11 and 19.08 times higher than that of single ring structure, respectively, while from the normalized transversal profiles (Figure 4c) all curves almost overlap with each other, indicating the plasmonic focal spot size remains the same. The strong spatial confinement with higher field enhancement is very attractive for near-field optical imaging and sensing in material characterization and biological applications.

A finite element method (COMSOL) model was developed to numerically investigate the focusing properties of the annular ring plasmonic lens under radially polarized il-

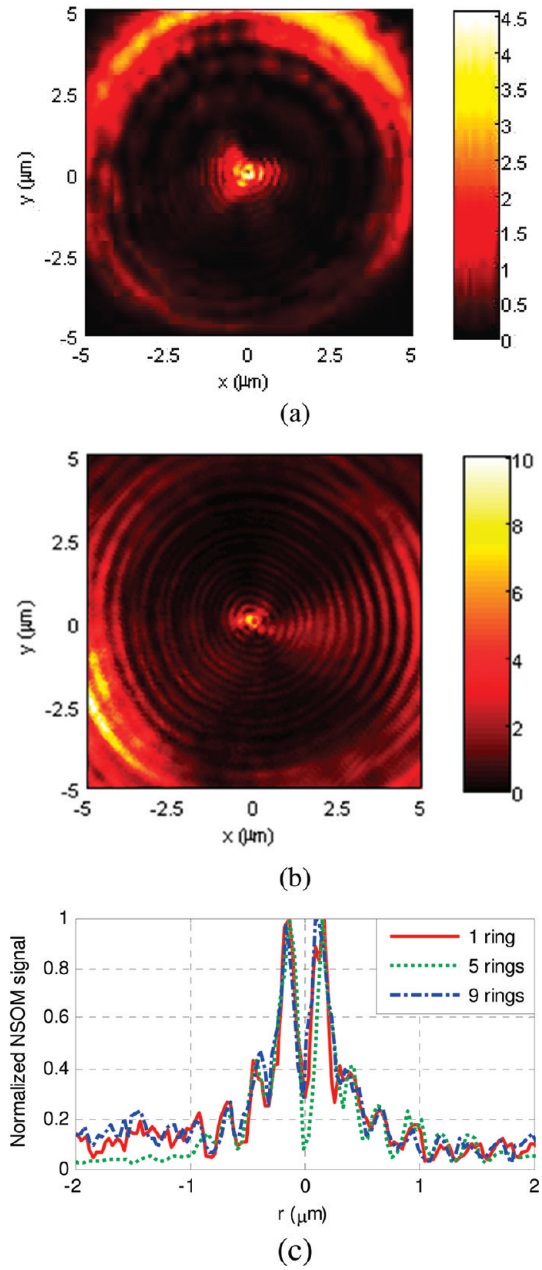

Figure 4. Measured near field energy density distribution at the air/silver interface for 5-ring (a) and 9-ring (b) plasmonic lens. The peak intensity of the plasmonic focus for 5-ring and 9-ring plasmonic lens is 8.11 and 19.08 times higher than that of single ring, respectively. (c) Comparison of measured normalized transverse profiles of energy density distribution for single ring, 5-ring, and 9 ring plasmonic lenses. These curves overlap each other, indicating that the focal spot remains the same.

lumination. Three-dimensional (3D) axially symmetric module was used to model the multiple concentric rings plasmonic lens as well as the optical excitation geometry. As an example, the calculated energy density distribution of a plasmonic lens with three concentric slits is illustrated in Figure 5. Since both the structure and the illumination are rotational symmetry, only half of the plasmonic lens structure is shown. The color represents the strength of the total field. The electric vector field arrows illustrate the local polarization pattern with longitudinal polarization pointing

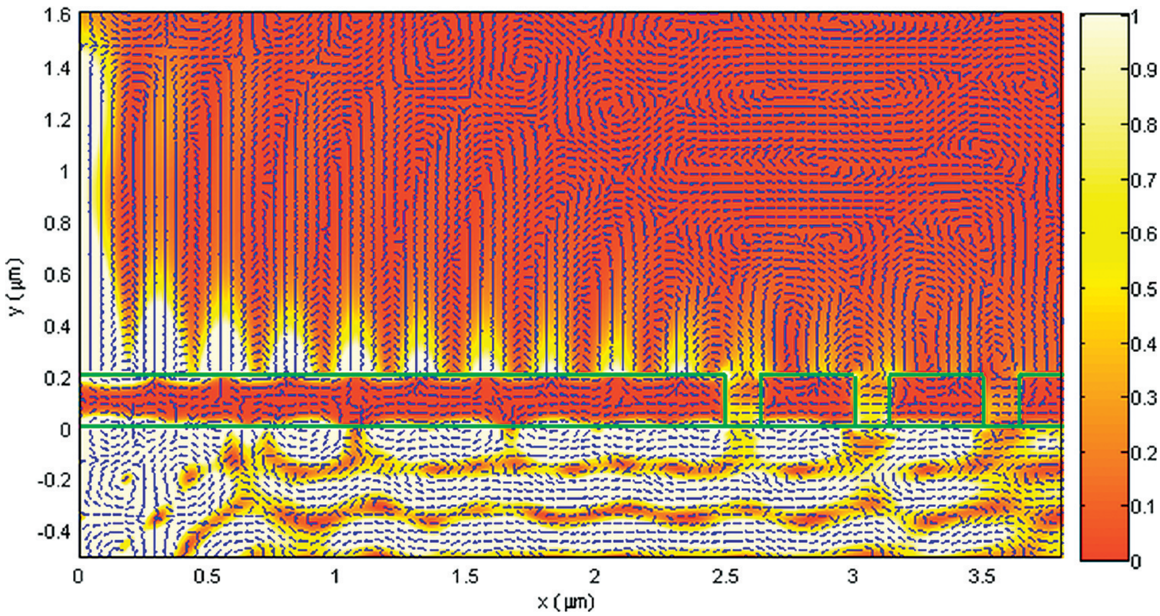

Figure 5. Illustration of a plasmonic lens with three concentric rings etched into silver film on glass with a slice of the computed plasmonic field. Details of the computed electric field and the electric vector field distributions are shown. Polarization vortex structures can be clearly identified near the slits.

at the vertical direction and radial polarization pointing at the horizontal direction. From the numerical simulation results, the electrical field distribution inside of the metal film clearly confirms the electron density oscillation at the metal dielectric interface. There are several other interesting features that are worthy of noticing here. The electric field near the vicinity of the focus are purely polarized along the longitudinal direction that is normal to the plasmonic lens surface, generating a kind of optical "needle" field similar to that reported recently using a combination of multiple zone diffractive optical element (DOE) and high NA objective lens.[21] The flat plasmonic lens provides a much more compact and simpler alternative to this approach. In addition, on both sides of the plasmonic lens the vector electric field shows polarization vortex structures near the slits that are worthy of further investigation.

From Figure 5, it is also observed that the side lobes "bend" outward as the observation planes moving farther away from the plasmonic lens surface, even though the field intensity gets much weaker. This phenomenon is due to the contributions of radiative fields that will lead to bigger spot size and fringe spacing. Strongly enhanced plasmonic fields dominates in the near field, while in the far field, radiative fields created at the subwavelength slits start to contribute to the total field distribution. This phenomenon is also experimentally verified. The decay length of surface plasmon in the direction that is normal to the surface is calculated to be 254.4 nm. To map the far field energy density distribution, the NSOM probe is retracted 2 μm away from the surface and the measured result is shown in Figure 6. The two peaks are about 346 nm away, corresponding to a fwhm spot size of 214 nm ($\sim\lambda/2.49$), which is larger than the corresponding result in the near field.

We further investigate the field enhancement factor of a single ring plasmonic lens with respect to its ring radius r.

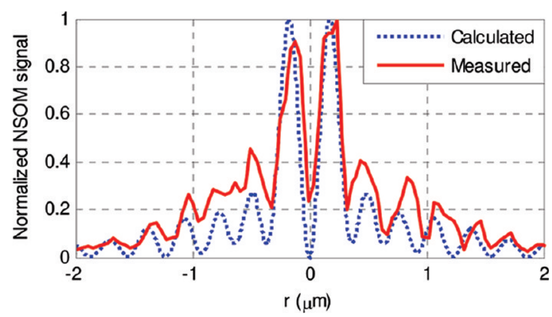

Figure 6. Comparison of measured and calculated far field transverse profiles of energy density distributions with the NSOM probe retracted 2 μm away from the surface. Radiative fields start to contribute to the total energy density distribution.

First, in the finite element model, the illumination is set to be radially polarized beam with uniform amplitude distribution and the metallic slit width d is chosen to be 135 nm. Then the ring radius r is varied from 1 to 50 μm with a step size of 0.5 μm. The result of this study is shown in Figure 7. It is found that the highest field enhancement is about 6.50 with optimal ring radius of 8.47 μm. The field enhancement can be further improved through adjusting the slit width d, while the field enhancement curve with respect to radius r maintains the same envelope. This is illustrated by an example for slit width d = 200 nm (also shown in Figure 7). The surface plasmon polaritons excited at the edge of the annular ring should be proportional to its perimeter $2\pi \cdot r$. Therefore, the surface plasmon intensity has a linear dependence on r, and the field enhancement factor should be proportional to $r^{0.5}$. The surface plasmons excited at all azimuthal directions propagate along the air−silver interface to the center of the plasmonic lens with a propagation loss of $\exp[-\mathrm{Im}(k_{sp}) \cdot r]$, where

$$k_{sp} = \frac{2\pi}{\lambda}\sqrt{\frac{\varepsilon_1\varepsilon_2}{\varepsilon_1 + \varepsilon_2}} \quad (1)$$

Here, ε_1 and ε_2 are dielectric constants of air and silver film, respectively, and ε_2 is chosen to be $-10.1786 + 0.8238i$ for the excitation wavelength of 532 nm.[22] Therefore, the analytical expression for the field enhancement factor E_{fe} is proportional to $r^{0.5} \times \exp[-\mathrm{Im}(k_{sp})\cdot r]$. This analytical expression is illustrated along with the numerically simulated field enhancement factor in Figure 7, where an excellent agreement between the analytical and numerical methods has been obtained. The field enhancement factor gradually approaches zero as ring radius increases due to propagation loss along the air–silver interface.

In practice, the incident light has certain field distribution pattern and spot size. The field enhancement of a plasmonic lens can be optimized through designing multiple concentric rings structure matching to the illumination spot. For example, the radially polarized illumination has donut shape field distribution of $E_{in} = r\cdot\exp(-r^2/w^2)$, where w is the beam waist and is assumed to be 3 μm in the following calculation. The overlapping field enhancement profile E_p for this illumination can be expressed as $E_p = E_{fe} \times E_{in}$ (Figure 8a). From Figure 8a, one can see the optimal location for a single ring is $r = 2.48$ μm, as opposed to the 8.47 μm optimal radius under uniform amplitude illumination. Then the field enhancement can be maximized for the single ring plasmonic lens through adjusting the ring width d. The maximum enhancement is found to be 8.4 with $d = 219$ nm. The field enhancement can be further improved by adding additional concentric rings if their locations are chosen to satisfy the circular Bragg condition for the plasmonic wavelength. From the field-enhancement profile, additional annular ring with radius r less than 8 μm can contribute to the total field enhancement. The benefit of adding more annular rings beyond 8 μm becomes negligible. Therefore, one can put additional rings in this radius range with their distance $n\cdot\lambda_{sp}$ to the first single ring, where n is an integer and λ_{sp} is the plasmonic wavelength of 510 nm. The maximum field enhancement is found to be 45.33 with a ring number of 11. The obtained plasmonic lens is optimal for the above illumination with field distribution $r\cdot\exp(-r^2/w^2)$ and $w = 3$ μm. The field-enhancement factor of the designed plasmonic lens varies if the illumination condition is changed. Figure 8b shows the relationship between the electric field-enhancement factor and beam waist w with the designed multiple concentric rings structure. It is found that there is an optimal beam waist of 3 μm for the plasmonic lens, which is where the plasmonic lens structure was optimized. This relationship also indicates that, given a fabricated multiple ring plasmonic lens, one may be able to conveniently maximize the enhancement effect by adjusting the size of the focal spot through controlling the focus of the objective lens.

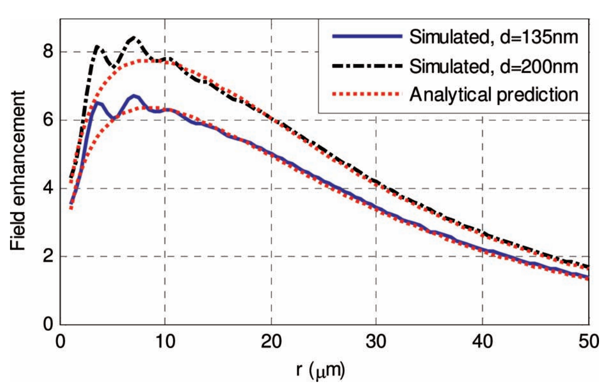

Figure 7. Numerically simulated field enhancement factor curves with respect to ring radius r for single ring plasmonic lens with different slit widths (135 and 200 nm, respectively) and their corresponding analytical predictions.

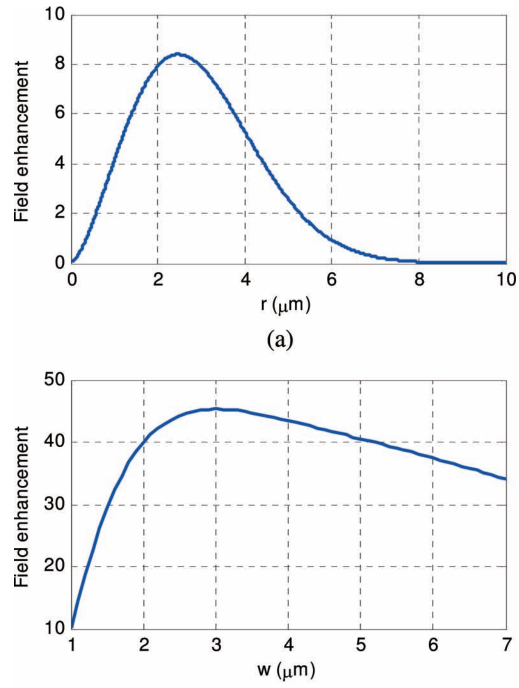

Figure 8. (a) Overall field-enhancement factor curve for single ring plasmonic lens when the field distribution of the illumination is taken into consideration. (b) Field-enhancement factor curve for a multiple ring plasmonic lens optimized at 3 μm illumination beam waist under the illumination of radial polarization with different beam waist sizes w.

In conclusion, optimal plasmonic focusing has been studied for plasmonic lens with single circular slit as well as multiple concentric slits carved into metal thin film. Under a radially polarized beam illumination, the entire beam is TM polarized with respect to the plasmonic lens structure. Surface plasmon waves excited by the radially polarized light propagate toward the center of plasmonic lenses and constructively interfere to create a strongly enhanced focal spot with spot size beyond the diffraction limit ($\lambda/2.88$). The experimental results also confirmed that the peak intensity of the plasmonic focus can be further enhanced while maintaining the focal spot size by adding more concentric rings that satisfy the circular Bragg condition for the plasmonic wavelength. Strategy for optimizing the field enhancement factor is also presented with both analytical and numerical methods. The plasmonic focal field created this way is an evanescent optical

"needle" field with the electric field substantially polarized normal to the flat plasmonic lens surface. Such a unique plasmonic focal field offers tremendous advantages in terms of the plasmonic focus shape, peak intensity, and spatial localization that may find broad applications in near-field imaging, sensing, lithography and nanoparticle manipulations, etc.

References

(1) Barnes, W. L.; Dereux, A.; Ebbersen, T. W. *Nature* **2003**, *424*, 824–830.
(2) Ozbay, E. *Science* **2006**, *311*, 189–193.
(3) Fang, N.; Lee, H.; Sun, C.; Zhang, X. *Science* **2005**, *308*, 534–537.
(4) Liu, Z.; Lee, H.; Xiong, Y.; Sun, C.; Zhang, X. *Science* **2007**, *315*, 1686.
(5) Smolyaninov, I. I.; Hung, Y.; Davis, C. C. *Science* **2007**, *315*, 1699–1701.
(6) Srituravanich, W.; Pan, L.; Wang, Y.; Sun, C.; Bogy, D. B.; Zhang, X. *Nat. Nanotechnol.* **2008**, *3*, 733–737.
(7) Kim, S.; Jin, J.; Kim, Y.-J.; Park, I.-Y.; Kim, Y.; Kim, S.-W. *Nature* **2008**, *453*, 757–760.
(8) Bozhevolnyi, S. I.; Volkov, V. S.; Devaux, E.; Laluet, J.; Ebbesen, T. W. *Nature* **2006**, *440*, 508–511.
(9) Rothenhäusler, B.; Knoll, W. *Nature* **1988**, *332*, 615–617.
(10) Liu, Z. W.; Steele, J. M.; Srituravanich, W.; Pikus, Y.; Sun, C.; Zhang, X. *Nano Lett.* **2005**, *5*, 1726–1729.
(11) Bouhelier, A.; Ignatovich, F.; Bruyant, A.; Huang, C.; Colas Des Francs, G.; Weeber, J.-C.; Dereux, A.; Wiederrecht, G. P.; Novotny, L. *Opt. Lett.* **2007**, *32*, 2535–2537.
(12) Zhan, Q. *Opt. Lett.* **2006**, *31*, 1726–1728.
(13) Chen, W.; Zhan, Q. *Proc. SPIE* **2007**, *6450*, 64500D.
(14) Chen, W.; Zhan, Q. *Opt. Express* **2007**, *15*, 4106–4111.
(15) Chen, W.; Zhan, Q. *Opt. Lett.* **2009**, *34*, 722–724.
(16) Lerman, G. M.; Yanai, A.; Levy, U. *Nano Lett.* **2009**, *9*, 2139–2143.
(17) Youngworth, K. S.; Brown, T. G. *Opt. Express* **2000**, *7*, 77–87.
(18) Zhan, Q.; Leger, J. R. *Opt. Express* **2002**, *10*, 324–331.
(19) Sun, C.; Liu, C. *Opt. Lett.* **2003**, *28*, 99–101.
(20) Novotny, L.; Hecht, B. *Principles of nano-optics*; Cambridge Univ. Press: Cambridge, MA, 2006.
(21) Wang, H. F.; Shi, L. P.; Lukyanchuk, B.; Sheppard, C.; Chong, C. T. *Nat. Photonics* **2008**, *2*, 501–505.
(22) Palik, E. D. *Handbook of Optical Constants of Solids*; Academic Press: San Diego, CA, 1998.

NL903145P